SUPPLEMENTAL FIGURES AND LEGENDS

Figure S1

A

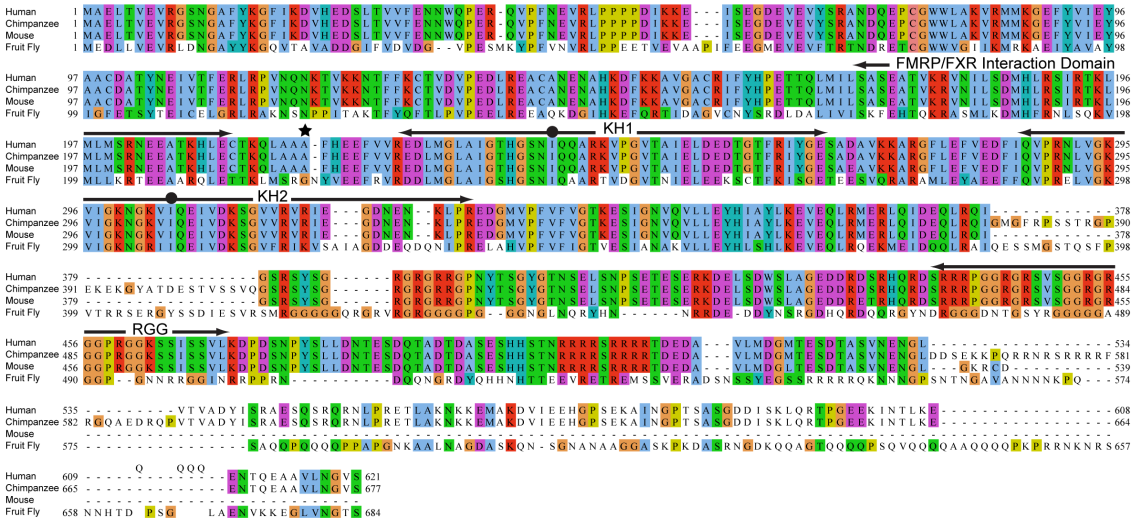

B

Position	Length	Potential G-quadruplex Forming Sequence	G-Score
32	29	**GG**AAAC**GG**AUGAUAACU**GG**UCCGCAGU**GG**	16
238	26	**GG**UAUG**GG**CAAAUCA**GG**CAAAUCU**GG**	18
352	25	**GG**CCAUGAUU**GGGG**UGCUUGUUU**GG**	12

C

AUGACUUCGAAAGUUUAUGAUCCAGAACAAAGGAAACGGAUGAUAACUGGUCCGCAGUGGUGGGCCAGAUGUAAACA
AAUGAAUGUUCUUGAUUCAUUUAUUAAUUAUUAUGAUUCAGAAAAACAUGCAGAAAAUGCUGUUAUUUUUUUACAUGG
UAACGCGGCCUCUUCUUAUUUAUGGCGACAUGUUGUGCCACAUAUUGAGCCAGUAGCGCGGUGUAUUAUACCAGAC
CUUAUUGGUAUGGGCAAAUCAGGCAAAUCUGGUAAUGGUUCUUAUAGGUUACUUGAUCAUUACAAAUAUCUUACUGC
AUGGUUUGAACUUCUUAAUUUACCAAAGAAGAUCAUUUUUGUCGGCCAUGAUUGGGGUGCUUGUUUGGCAUUUCAUU
AUAGCUAUGAGCAUCAAGAUAAGAUCAAAGCAAUAGUUCACGCUGAAAGUGUAGUAGAUGUGAUUGAAUCAUGGGAU
GAAUGGCCUGAUAUUGAAGAAGAUAUUGCGUUGAUCAAAUCUGAAGAAGGAGAAAAAAUGGUUUUGGAGAAUAACUU
CUUCGUGGAAACCAUGUUGCCAUCAAAAAUCAUGAGAAAGUUAGAACCAGAAGAAUUUGCAGCAUAUCUUGAACCAUU
CAAAGAGAAAGGUGAAGUUCGUCGUCCAACAUUAUCAUGGCCUCGUGAAAUCCCGUUAGUAAAAGGUGGUAAACCUG
ACGUUGUACAAAUUGUUAGGAAUUAUAAUGCUUAUCUACGUGCAAGUGAUGAUUUACCAAAAAUGUUUAUUGAAUCG
GACCCAGGAUUCUUUUCCAAUGCUAUUGUUGAAGGUGCCAAGAAGUUUCCUAAUACUGAAUUUGUCAAAGUAAAAGG
UCUUCAUUUUUCGCAAGAAGAUGCACCUGAUGAAAUGGGAAAAUAUAUCAAAUCGUUCGUUGAGCGAGUUCUCAAAA
AUGAACAAUAA

Figure S1. Amino acid sequence alignment of FMRP and FMRP binding sequences in *Renilla* luciferase mRNA (related to Figure 1). **(A)** The sequence of human, chimpanzee, mouse, and fruit fly FMRP were aligned using COBALT and displayed using JALVIEW. Previously identified functional domains of FMRP are indicated by the arrows and include the FMRP/FXR interaction domain, KH1, KH2, and RGG domains. The highly conserved isoleucine residues that are important for the function of the KH domains are indicated by the filled circles. The star indicates the N-terminus of NT-dFMRP. **(B)** Putative G-quadruplex forming sequences in *Renilla* luciferase mRNA. The mRNA sequence for *Renilla* luciferase from the start codon (position 1) to the stop codon (position 936) was analyzed using QGRS Mapper (Kikin et al., 2006). There are potentially 3 non-overlapping quadruplex forming G-rich sequences at the indicated positions with G-Scores ranging from 12 to 18. For comparison, the G-score for the well-studied SC-1 G-quadruplex (Darnell et al., 2001) forming sequence is 20. The guanines involved in G-quadruplex formation are indicated in bold and are underlined. **(C)** The sequence of *Renilla* luciferase mRNA showing the location of WGGA (magenta) and ACUK (green) sequences (in which W = A or U and K = G or U).

Figure S2

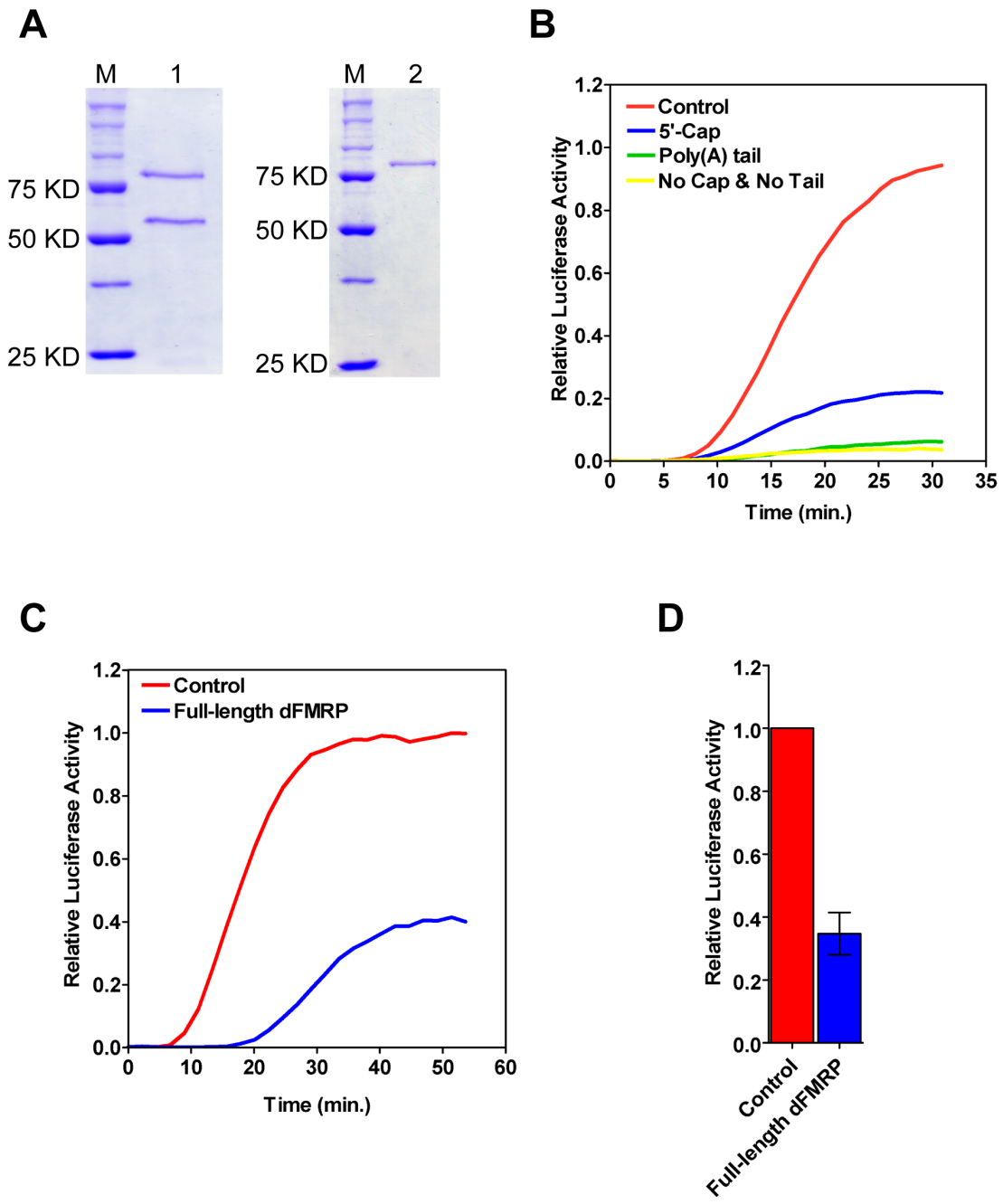

Figure S2. Purification of dFMRP and inhibition of translation (related to Figure 1). (A) SDS-PAGE showing that expression and purification of the full-length dFMRP results in the

truncation of about 50% of the protein by ≈20 KD. Mass spectrometry analysis showed that amino acids 1 to 119 are missing from the truncated dFMRP protein. The SDS-PAGE on the right shows the full-length dFMRP purified using a dual tag method (The first purification was done with a C-terminal chitin-binding domain and intein tag followed by a second purification with a N-terminal hexahistidine tag, which eliminates the truncated dFMRP). **(B)** Time course of luciferase mRNA translation. The *Drosophila* embryo extract *in vitro* translation system has the same selectivity for mRNA features as *in vivo* translation. Control (red trace), luciferase mRNA with a N^7-methyl guanosine cap at the 5' end and a 3'-poly(A) tail; 5'-Cap (blue trace), luciferase mRNA with a N^7-methyl guanosine cap at the 5' end but without a 3'-poly(A) tail; Poly(A) tail (green trace), luciferase mRNA with a 3'-poly(A) tail but with a N^7-methyl guanosine cap at the 5' end; No Cap & No Tail (yellow trace), luciferase mRNA without a N^7-methyl guanosine cap at the 5' end and without a 3'-poly(A) tail. **(C)** Inhibition of translation by full-length dFMRP. Red trace, control translation without dFMRP; blue trace, translation with 0.6 μM full-length dFMRP. **(D)** The bar graph shows the average inhibition by the full-length dFMRP and the standard deviations from two independent experiments. The data were normalized with respect to the control translation without dFMRP.

Figure S3

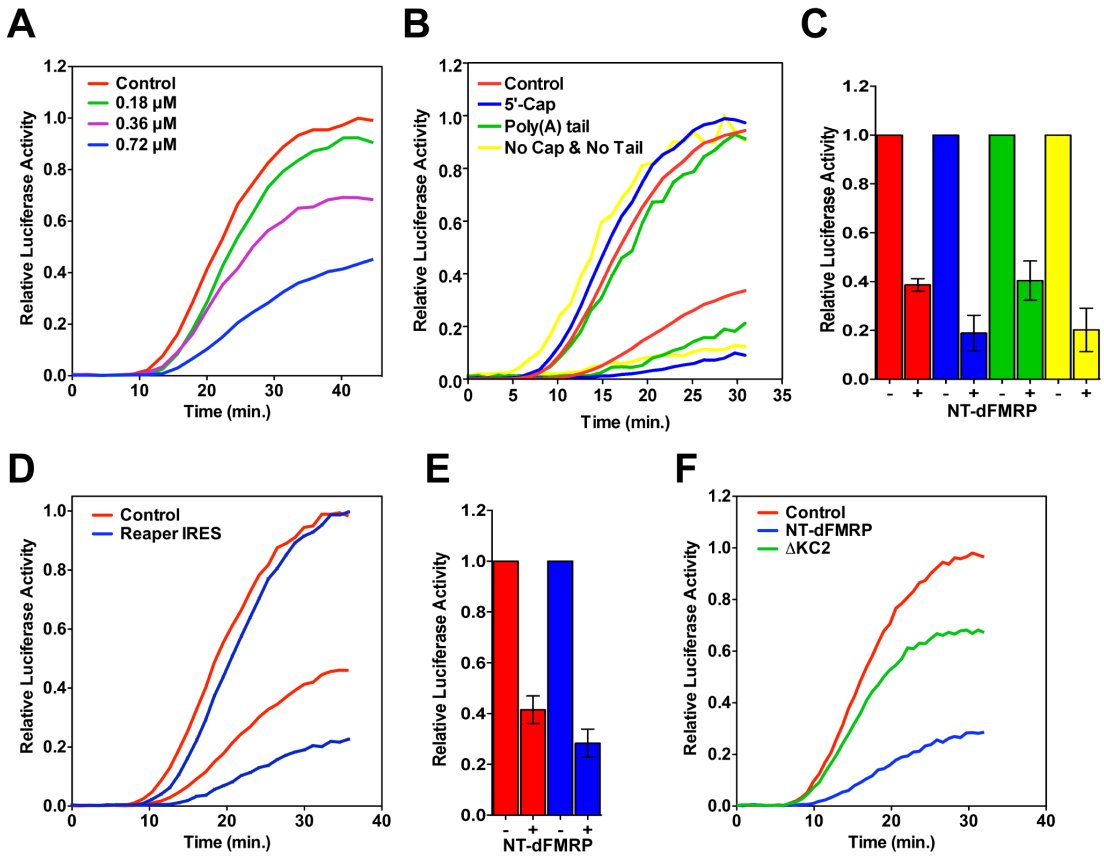

Figure S3. Inhibition of translation by FMRP is independent of 5'-Cap and 3'-poly (A) tail in the mRNA (related to Figure 1). (A) Time course of luciferase mRNA translation at different concentrations of NT-dFMRP. Red trace, control translation without NT-dFMRP; green trace, translation with 0.18 µM NT-dFMRP; purple trace, translation with 0.36 µM NT-dFMRP; blue trace, translation with 0.72 µM NT-dFMRP. **(B)** The 5'-cap and 3'-poly (A) tail of the mRNA are not required for translational repression by NT-dFMRP. Red trace, translation of mRNA having 5'-cap and 3'-poly (A) tail; blue trace, translation of mRNA without the 5'-cap; green trace, translation of mRNA without the 3'-poly (A) tail; yellow trace, translation of mRNA without the 5'-cap and the 3'-poly (A) tail. All traces were normalized by setting the highest signal obtained without NT-dFMRP to 1. The lower traces are the same mRNAs translated in the presence of 0.6

μM NT-dFMRP and were normalized with respect to identical reactions performed in the absence of NT-dFMRP. **(D)** Inhibition of IRES-dependent translation by FMRP. Red trace, control mRNA; blue trace, mRNA with the reaper IRES at the 5'-UTR of luciferase mRNA. The lower traces are the same mRNAs translated in the presence of 0.6 μM NT-dFMRP. The data were normalized with respect to the control mRNA translation without NT-dFMRP. **(F)** Inhibition of translation by NT-dFMRP is reversible. Red trace, control translation without NT-dFMRP; blue trace, translation with 0.6 μM NT-dFMRP; green trace, translation with 0.6 μM NT-dFMRP and 1.5 μM of ΔKC2 RNA added in trans to the in vitro translation reaction. The bar graphs in **(C)** and **(E)** show the standard deviations from three independent experiments and are color coded as the respective time courses. - and + below the bar graphs indicate the absence and presence of NT-dFMRP in the reactions.

Figure S4

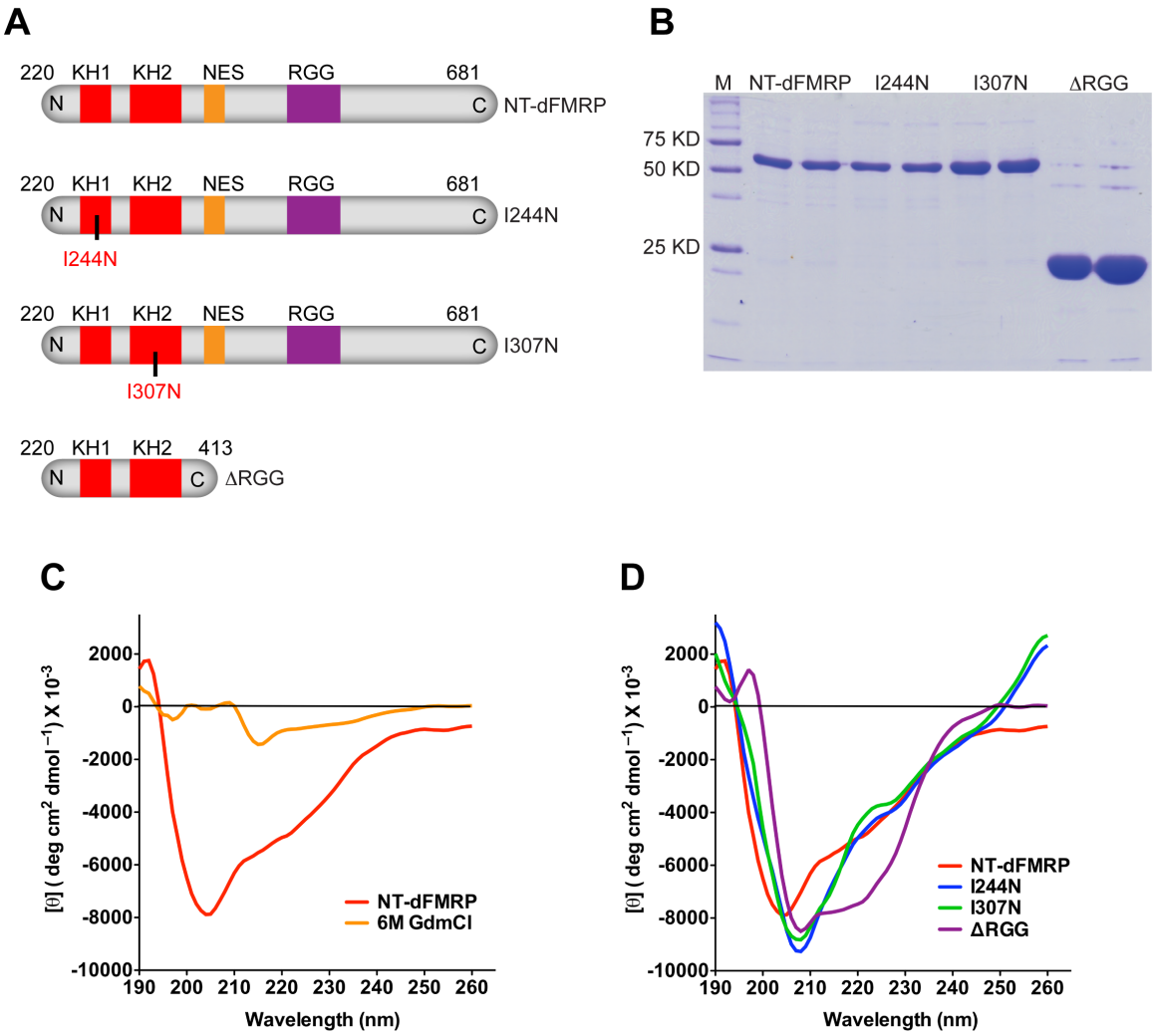

Figure S4. Purification of NT-dFMRP mutants (related to Figure 1). **(A)** Cartoon showing NT-dFMRP (220 to 681 amino acids), KH1 (I244N), KH2 (I307N) and ΔRGG (220 to 413 amino acids) mutants. **(B)** SDS-PAGE showing the purity of NT-dFMRP mutants. **(C)** Circular dichroism spectrum of NT-dFMRP. The CD scan of NT-dFMRP in the absence (red trace) and in the presence of 6M guanidium hydrochloride (orange trace) to unfold the protein are shown. **(D)** Circular dichroism spectra of NT-dFMRP mutants. The CD spectra of the mutant proteins show

minor differences, indicating that the mutations or the deletion does not completely unfold the proteins.

Figure S5

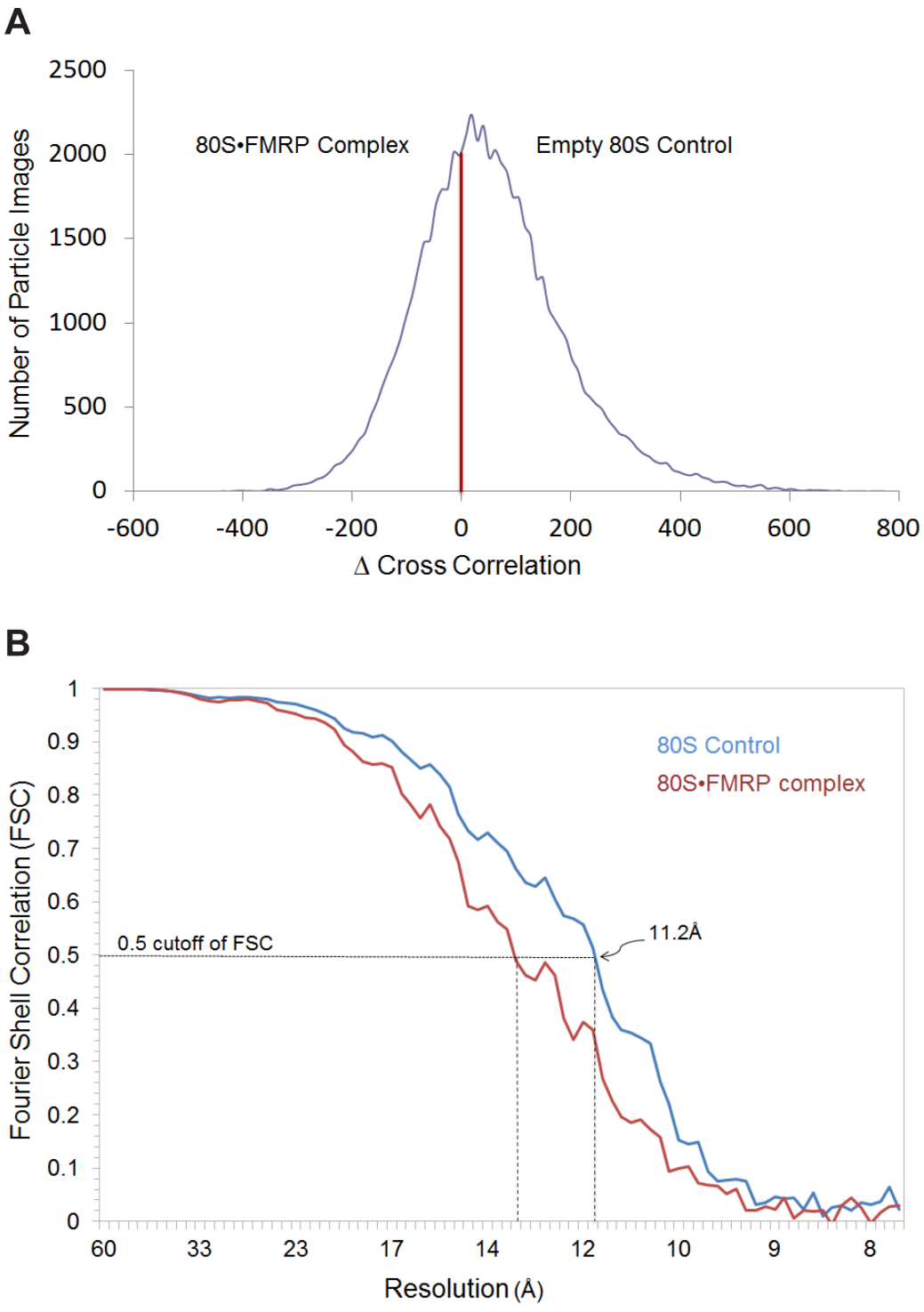
A
2500
2000
1500
1000
500
0
Number of Particle Images
80S•FMRP Complex
Empty 80S Control
-600
-400
-200
0
200
400
600
800
Δ Cross Correlation
B
1
0.9
0.8
0.7
0.6
0.5
0.4
0.3
0.2
0.1
0
Fourier Shell Correlation (FSC)
80S Control
80S•FMRP complex
0.5 cutoff of FSC
11.2Å
60
33
23
17
14
12
10
9
8
Resolution (Å)

Figure S5. Analysis of cryo-EM structure of 80S•FMRP complex (related to Figure 4). (**A**) Histogram obtained by supervised classification of particle images of the *Drosophila* 80S•FMRP complex. Values obtained by computing the difference between the cross-correlation coefficients (CCFs) of each experimental projection (image) of the 80S•FMRP complex with respect to two reference maps: (i) the original map of the 80S•FMRP complex, and (ii) the map of the empty 80S (control). Undecided images, equally dissimilar to the same computationally generated angular projections of either reference, are grouped around 0 on the X-axis, and indicated by a vertical red line. Differences in CCF values are expressed in arbitrary units. The number of images corresponding to each projection of the reference map is shown on the Y-axis. (**B**) Resolution curves for the cryo-EM maps of the control *Drosophila* 80S ribosome and the 80S•NT-dFMRP complex.

Figure S6

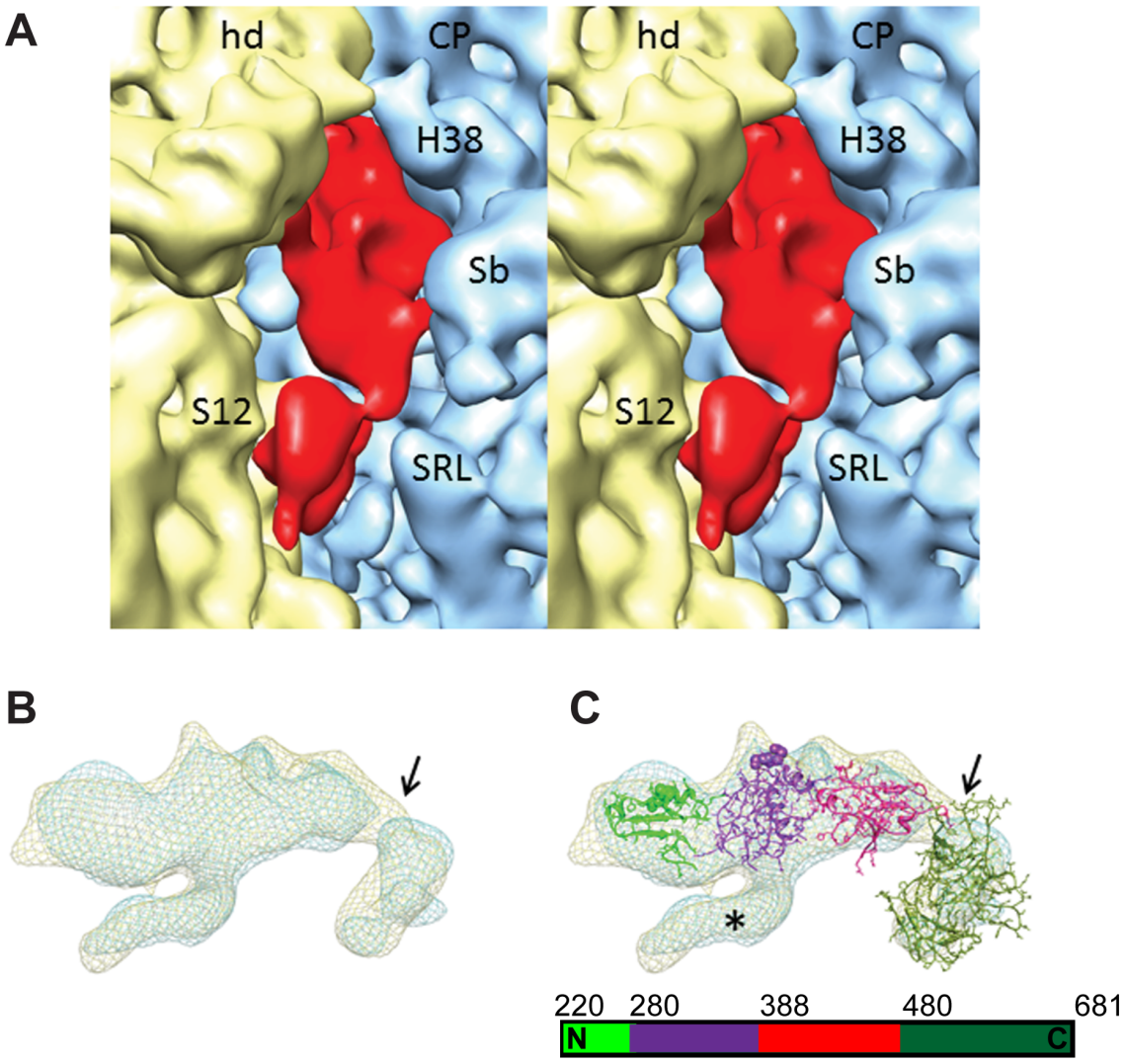

Figure S6. CryoEM structure of 80S•FMRP complex (related to Figure 4).

(A) A stereo view representation of the binding region of FMRP (red) on the *Drosophila* 80S ribosome. The orientation of the ribosome is same as in main Figure 4B. **(B)** A comparison of the cryo-EM densities corresponding to NT-dFMRP obtained before and

after supervised classification. Superimposed densities of the difference map (light yellow meshwork), obtained by subtracting the cryo-EM map of the 80S control from that of the 80S•NT-dFMRP complex (before classification), and segmented density corresponding to NT-dFMRP (light blue meshwork), as seen within the cryo-EM map computed from classified images. The arrow points to a region of absence of mass in the segmented density that could result due to flexibility of the NT-dFMRP's C-terminal domain (CTD). **(C)** Fitted positions of four structural domains of the NT-dFMRP homology model into the corresponding cryo-EM density. The space-filled segments within domains 1 (light green) and 2 (magenta) point to KH1 and KH2. As described in the Methods section, density corresponding to CTD is relatively week in both NT-dFMRP maps. In addition, we observe another week mass of unexplained density (marked with an asterisk [*] in panel (c). This density is situated next to the inter-subunit bridge (bridge B2a) forming segment (the helix 69 of the 28S rRNA within the 60S ribosomal subunit) and could result either from a conformational change in the helix 69 region or from an alternative conformation adopted by the FMRP in a small fraction of the ribosome population. Further characterization of this unexplained mass of density may be achieved through more rigorous classification using a much larger cryo-EM data set. A bar diagram depicting the four structural domains of the NT-dFMRP homology model in matching colors is shown at the lower right.

Figure S7

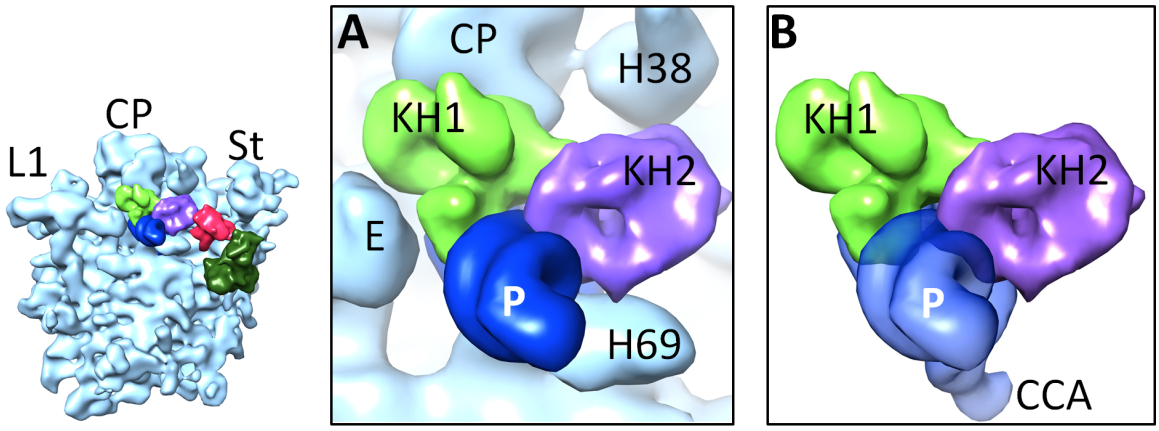

Figure S7: Superimposition of FMRP onto the ribosome-bound P-site tRNA (related to Figure 4). (**A**) Shown are the low-pass filtered, fitted coordinates of KH1 (green) and KH2 (purple) domains of FMRP that are color coded as in Figs. 4 and S6, along with the P-site tRNA (dark blue) (Armache et al., 2010). (**B**) Same as in panel A, but the ribosome density has been removed and tRNA is shown as semitransparent blue, to reveal the extent of overlaps between the anticodon arm of the tRNA and KH1 and KH2 domains of FMRP.

SUPPLEMENTAL REFERENCES

Armache, J.P., Jarasch, A., Anger, A.M., Villa, E., Becker, T., Bhushan, S., Jossinet, F., Habeck, M., Dindar, G., Franckenberg, S.*, et al.* (2010). Cryo-EM structure and rRNA model of a translating eukaryotic 80S ribosome at 5.5-A resolution. Proc Natl Acad Sci U S A *107*, 19748-19753.

Darnell, J.C., Jensen, K.B., Jin, P., Brown, V., Warren, S.T., and Darnell, R.B. (2001). Fragile X mental retardation protein targets G quartet mRNAs important for neuronal function. Cell *107*, 489-499.

Kikin, O., D'Antonio, L., and Bagga, P.S. (2006). QGRS Mapper: a web-based server for predicting G-quadruplexes in nucleotide sequences. Nucleic Acids Res *34*, W676-682.